Author's personal copy

Invest New Drugs
DOI 10.1007/s10637-015-0240-8

PRECLINICAL STUDIES

Screening and biological evaluation of myricetin as a multiple target inhibitor insulin, epidermal growth factor, and androgen receptor; in silico and in vitro

Pushpendra Singh[1] · **Felix Bast**[1]

Received: 24 January 2015 / Accepted: 7 April 2015
© Springer Science+Business Media New York 2015

Summary Myricetin is a naturally omnipresent benzo-α-pyrone flavonoids derivative; has potent anticancer activity. Receptor tyrosine kinases family provides the decisive role in cancer initiation and progression. These receptors have recently caught the attention of the researchers as an attractive target to combat cancer, owing to the evidences endorsed their over-expression on cancer cells. This study is a concerted effort to explore the potent and specific multi-targeted inhibitor against RTKs and AR\ER employing molecular docking approach. IR, IGF1R, EGFR, VEGFR1, VEGFR2, and AR\ER were chosen as a protein and natural compounds as a ligand. Molecular docking procedure followed by using Maestro 9.6 (Schrödinger Inc). All natural compounds were docked with the X-ray crystal structures of selected proteins by employing grid-based ligand docking with energetics Maestro 9.6. IBS natural compounds docked with each selected protein molecules by using GLIDE high throughput virtual screening. On the basis of Gscore, we selected 20 compounds from IBS (50,000 compounds) along with 68 anticancer compounds from published literature for GLIDE extra precision molecular docking. Calculated docking free energy yielded the excellent dock score for the myricetin when docked with proteins EGFR, IR, and AR\ER. Protein-ligand interactions profile highlighted that the lipophilic, hydrogen bonding and π-π stacking interactions play a central role in protein-ligand interactions at the active site. The results of MTT assay reveal that the myricetin inhibit the viability and proliferation of cancer cells in a dose-dependent manner. Treatment with the myricetin led to down-regulation of mRNA expression of EGFR, IR, mTOR, and Bcl-2. Although, further in vitro and in vivo experimental studies are required for the experimental validation of our findings.

Keywords Receptor tyrosine kinases · Androgen receptor/Estrogen receptor · Natural compounds · Cancer · Maestro 9.6

Introduction

Myricetin is a naturally occurring phenolic flavonol, found in red wine, many grapes, berries, fruits, vegetables and herbs possessing antioxidant properties. In vitro, investigations demonstrate that the myricetin in high concentrations can improve lipoproteins such as low-density lipoprotein cholesterol. Tyrosine kinase receptors (RTKs) are a trans-membrane receptor regulates a number of cellular activity including cell migration, adhesion, apoptosis, and cell proliferation. Overexpression or overactivity of RTKs has been reported in a diverse of cancers, including prostate, breast, lung and ovarian cancers. RTKs comprise of many proteins including insulin, IGF1, EGF, and VEGF receptors. Cell-membrane EGFR over-expressed and over activated in various cancers, including non-small cell lung, head and neck, breast and prostate cancers [1–5]. RTK class II (Insulin receptor family) Insulin and insulin growth factor have 40–80 % homology, so it is arduous to delineate insulin and IGF1 ligand-receptor interaction entirely. Insulin and IGF1 binds to IGF1R, IR-A, and hybrid receptors of IGF and IR-A mediates the mitogenic signaling pathway [6, 7] while ligand binding to IRB activates metabolic signaling [8]. Isoforms of IR (IR-A and IR-B) expression in the verity of human cancer cells including prostate, breast, osteosarcoma, non-small-cell lung carcinoma and acute myelogenous leukemia resulted from post-

✉ Felix Bast
felix.bast@gmail.com; felix.bast@cup.ac.in

[1] Centre for Biosciences, School of Basic and Applied Sciences, Central University of Punjab, Bathinda, Punjab, India 151001

Published online: 19 April 2015

Author's personal copy

transcriptional alternative splicing of insulin receptor [9–14]. The auto-phosphorylation and trans-phosphorylation of receptor cytoplasmic tyrosine residues lead to the recruitment of intracellular appurtenance protein molecules such as Grb2 and c-Src. These protein molecules commence an avalanche of intracellular signaling events that prompt diverse biological responses such as metabolism, cell proliferation, cell differentiation, cell-survival, and cell growth [15]. Ultimately phosphorylation of receptor recruits the downstream signaling protein IR substrate (IRS) 1 to 3 to the cell membrane, which eventually activates both phosphoinositide 3-kinase (PI3K), Akt, and the mitogen-activated protein kinase (MAPK) pathways.

Myricetin induced apoptosis, by decreasing the activity of PI3K in primary and metastatic pancreatic cancer cells. In silico result, also shows myricetin, quercetin, and luteolin have a better Gscore when docked with PI3K protein molecules [16]. Moreover, myricetin was recognized as dual-effective inhibitors for wild-Type EGFR and mutated EGFR by using in silico molecular docking protocol [17]. Furthermore, in-vivo, treatment of myricetin orthotopic pancreatic tumors, increases the tumor regression and decreased metastatic spread [18]. Myricetin-induced apoptosis by modulating the metabolic PI3K and mitogenic p38 MAPK signaling pathways on T24 and HepG2 Cells [19, 20]. Moreover, myricetin sturdily inhibited MEK1 kinase activity and suppressed TPA or EGF-induced phosphorylation of extracellular signal-regulated kinase (ERK) eventually led induce apoptosis and decreased cell proliferation [21]. However, the efficacy of myricetin as an anticancer agent in lung and prostate cancer is unknown. Therefore, in the present communication, we studied to investigate the effect of myricetin on cancer cell growth and apoptosis by using in silico and in vitro.

Materials and methods

In silico methodology

Selection of ligand and protein molecules

In silico molecular docking protocol accommodated from our previous published article [17, 16, 22]. The schematic workflow of screening of multitargeted compound and biological effect in cancer cell lines was illustrated in Fig. 1. Ligand dataset were selected in our study, a) Inter BioScreen natural compound library (IBS), and b) Anticancer natural compounds that have been reported in the publish literature [23–28]. List of anticancer natural compounds (PubChem ID) screened in this study with structural and physicochemical parameters presented in Table 1. All selected ligands were subjected to Ligprep wizard application of the Maestro 9.6 (Schrödinger Inc). Ligprep performs many corrections on

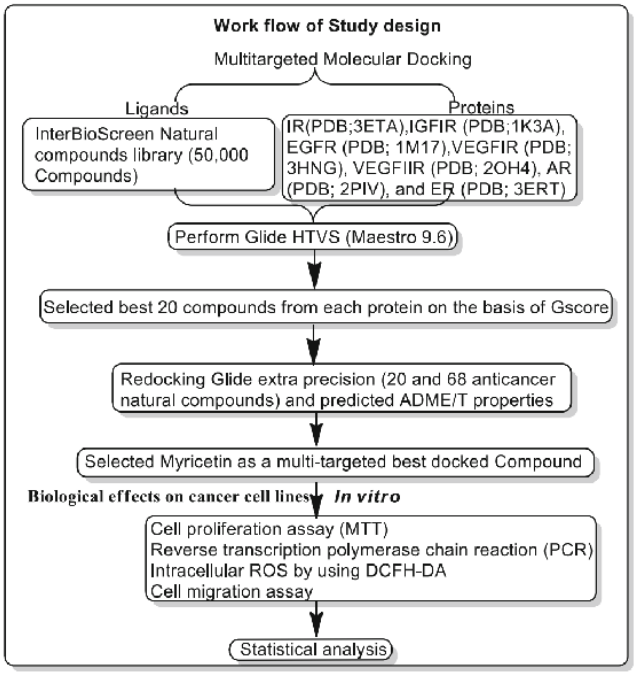

Fig. 1 Workflow of Screening of multitargeted compound (myricetin) and biological effect in cancer cell lines (study design)

the ligands, such as the addition of hydrogens, 2D to 3D conversion, corrected bond lengths and bond angles, low energy structure, stereochemistries and ring conformation. Apart from that another parameter such as ionization does not change, tautomers not generated and retain specific charities generate at most one per ligands were used as a default parameter in Maestro 9.6. The X-ray crystal structure of IR (PDB; 3ETA), IGFIR (PDB; 1K3A), EGFR (PDB; 1M17), VEGFR1 (PDB; 3HNG), VEGFR2 (PDB; 2OH4), AR (PDB; 2PIV), and ER (PDB; 3ERT) retrieved from the protein data bank. Maestro 9.6 protein preparation wizard application performed for the correction of raw PDB structure; these are the addition of hydrogen atoms, assigning bond orders and bond length, creation of zero order bonds to metal, creation of disulphide bonds, fixing of the charges and orientation of groups were incorporated in to the protein.

Molecular docking

Molecular docking studies using the selected ligand molecules were conducted using Maestro 9.6 molecular docking suite [29–31]. Each of these compounds was docked into different target protein molecules, and the docking conformation possessing the lowest energy was stipulated. Input ligands and protein molecules were prepared using respective wizard applications of Maestro 9.6. In addition, optimized potential for liquid simulations (OPLS_2005) force field applied for local energy minimization (bond stretching energy) and geometry optimization [32–34]. Finally, one conformation for

Author's personal copy

Table 1 List of PubChem molecules screened in this study with Structural and physicochemical Parameters (16)

S.N.	Comp. (CID)	Mol. Wt. (130–725)	Volume (500 to 2000)	H-bond Donor (0–6)	H-Bond Accp. (2–20)	QPlogP oct (8.0 to 35.0)	QPlog Pw (4.0 to 45.0)	QPlog $P_{o/w}$ (−2.0-6.5)	QPlogS mol/L (−6.5 to 0.5).
1	176,870	393.441	1226.24	1.5	7.4	18.347	10.736	3.942	−4.335
2	101,84653	485.945	1449.822	2	9.45	25.015	14.39	3.847	−5.269
3	208,908	581.06	1674.641	1	8.25	26.434	13.376	5.881	−6.837
4	5,328,779	294.309	980.124	3	5.5	17.809	12.771	1.849	−4.481
5	123,631	446.908	1262.744	1	7.7	19.692	10.252	3.898	−3.559
6	932	272.257	840.858	2	4	14.728	10.219	1.658	−3.47
7	2044	305.173	871.406	1	3.75	12.522	6.462	2.434	−4.415
8	2543	310.435	1122.807	1	1.5	13.745	4.396	5.604	−6.637
9	3220	270.241	808.031	1	4.25	12.607	8.522	1.258	−3.07
10	5350	177.279	661.995	0	6.5	9.242	8.882	0.535	0.827
11	73,641	488.706	1431.329	4	7.1	25.992	14.438	4.231	−5.37
12	73,659	472.707	1414.592	3	5.4	23.674	11.514	5.168	−6.242
13	91,469	242.274	798.666	2	2.25	13.082	8.215	2.761	−3.579
14	245,005	645.745	1754.494	3	16.95	33.013	22.138	1.963	−2.418
15	259,846	426.724	1378.31	1	1.7	17.885	4.492	7.043	−7.907
16	261,265	430.626	1387.41	2	6.15	21.018	10.026	4.381	−6.176
17	440,917	136.236	621.544	0	0	5.044	−0.203	3.99	−4.003
18	441,794	496.553	1351.712	5	12.35	28.735	20.523	1.144	−3.268
19	442,793	294.39	1090.905	1	4.2	13.232	5.745	3.766	−4.42
20	445,154	228.247	786.572	3	2.25	13.599	9.347	2.012	−2.803
21	9064	290.272	872.256	5	5.45	19.89	15.596	0.481	−2.609
22	10,494	456.707	1401.838	2	3.7	21.162	8.308	6.238	−7.067
23	16,078	314.467	1147.852	1	1.5	13.759	3.962	5.694	−6.774
24	64,945	456.707	1387.747	2	3.7	20.965	8.275	6.125	−6.917
25	65,064	458.378	1255.716	8	8.75	31.171	23.925	−0.24	−3.547
26	68,077	372.374	1098.572	0	6.25	15.512	7.736	3.31	−3.466
27	72,276	290.272	872.747	5	5.45	19.683	15.562	0.494	−2.587
28	72,277	306.271	892.592	6	6.2	21.772	17.64	−0.17	−2.356
29	72,281	302.283	919.955	2	4.75	15.742	10.473	1.803	−3.782
30	72,326	442.724	1393.324	2	3.4	20.187	7.483	5.92	−6.784
31	446,925	536.882	2240.509	0	0	21.45	−4.618	19.06	−21.136
32	457,964	338.486	1040.152	4	5.85	19.237	12.383	1.916	−3.138
33	3,035,241	323.822	1004.466	2.5	6.25	17.869	11.099	2.03	−2.845
34	5,270,604	426.724	1374.435	1	1.7	18.141	4.741	7.024	−8.012
35	5,280,343	302.24	883.724	4	5.25	18.67	14.544	0.522	−3.1
36	5,280,373	284.268	860.146	1	3.75	13.02	8.02	2.522	−3.523
37	5,280,443	270.241	822.143	2	3.75	14.898	10.217	1.644	−3.374
38	5,280,445	286.24	843.558	3	4.5	16.591	12.301	0.96	−3.096
39	5,280,789	538.898	2258.34	0	0	21.818	−4.468	19.12	−21.322
40	5,280,863	286.24	840.186	3	4.5	16.394	12.278	1.059	−3.057
41	5,280,896	264.321	879.908	2	4.75	13.913	8.701	2.18	−2.772
42	5,280,899	568.881	2125.203	2	3.4	25.936	5.687	10.56	−12.471
43	5,280,961	270.241	807.798	2	3.75	14.142	9.887	1.678	−3.014
44	5,281,605	270.241	818.653	2	3.75	15.089	10.185	1.757	−3.317
45	5,281,607	254.242	799.678	1	3	12.869	8.121	2.386	−3.647
46	5,281,612	300.267	901.458	2	4.5	15.652	10.473	1.79	−3.694
47	5,281,614	286.24	841.842	4	5.5	18.889	14.744	0.5	−2.796

Author's personal copy

Table 1 (continued)

S.N.	Comp. (CID)	Mol. Wt. (130–725)	Volume (500 to 2000)	H-bond Donor (0–6)	H-Bond Accp. (2–20)	QPlogP oct (8.0 to 35.0)	QPlog Pw (4.0 to 45.0)	QPlog $P_{o/w}$ (−2.0-6.5)	QPlogS mol/L (−6.5 to 0.5).
48	5,281,616	270.241	817.4	2	3.75	14.551	10.181	1.794	−3.308
49	5,281,670	302.24	858.752	4	5.25	19.268	14.332	0.41	−2.755
50	5,281,672	318.239	882.348	5	6	20.432	16.443	−0.28	−2.564
51	6,917,781	805.013	2188.868	5	14.05	39.445	21.319	6.229	−6.364
52	9,548,699	274.489	963.039	0	0	9.861	−0.523	8.186	−8.689
53	9,548,711	278.52	1081.566	0	0	10.365	−1.273	9.272	−9.918
54	9,825,149	453.586	1502.475	2	5.25	23.868	11.935	5.735	−7.262
55	9,910,986	401.846	1141.405	2	6.7	20.745	12.793	2.369	−3.673
56	5,281,707	268.225	774.132	2	4.5	14.593	10.923	1.319	−2.915
57	5,281,708	254.242	787.865	2	4	14.141	10.264	1.774	−2.957
58	6,436,722	542.93	2281.771	0	0	22.431	−4.283	18.96	−21.565
59	6,441,009	785.023	2136.644	9	21.15	48.098	33.717	1.359	−2.85
60	6,857,485	276.504	1033.576	0	0	10.507	−0.266	8.832	−9.421
61	1,135,3973	479.965	1419.846	2	6.4	24.197	12.538	5.001	−7.537
62	1,147,6171	439.559	1456.758	2	3.25	22.132	9.911	6.748	−8.739
63	11,640,390	421.501	1336.398	3	4.75	24.019	13.923	5.015	−7.393
64	2,478,5538	461.501	1398.675	3	7.5	26.47	15.152	4.164	−6.935
65	4,688,1851	439.559	1458.756	2	3.25	22.144	9.957	6.742	−8.831
67	5,660,3750	678.82	1960.352	8	14	41.827	28.302	2.644	−5.369
68	57,390,076	515.66	1691.49	4	8	29.212	15.987	4.552	−6.261

Compounds; PubChem molecules screened in this study

Molecular weight (<500 Da)

Volume; Estimated number of hydrogen bonds that would be accepted by the solute from water molecules in an aqueous solution. Values are averages taken over a number of configurations, so they can be non-integer

Hydrogen bond donors (<5)

Hydrogen bond acceptors (<10)

QP log Poct; was predicted partition coefficient of octanol/gas, (8.0 to 35.0)

QP log Pw; was predicted partition coefficient of water/gas (4.0 to 45.0)

Plog Pw; was Predicted octanol/water partition co-efficient log p (recommended range: −2.0 to 6.5)

QPlog S; was Predicted aqueous solubility; S in mol/L (acceptable range: −6.5 to 0.5)

each ligand was prompt for molecular docking protocol. After the execution of ligands and protein preparation, a receptor-grid file was generated. Van der Waal radii of receptor atom by 1.00 Å and a partial atomic charge of 0.25 scaled for the generation of the receptor grid. The active site of the receptor provides an accurate scoring function with thermodynamically optimal energy and is calculated on a grid by various sets of fields. After the generation of receptor-grid file, molecular docking was performed. HTVS was performed using the GLIDE docking module within the Schrödinger Suite. All natural compounds were docked with the X-ray crystal structures of selected proteins by employing grid-based ligand docking with energetics Maestro 9.6. IBS natural compounds docked with each selected protein molecules by using GLIDE high throughput virtual screening. On the basis of Gscore, we selected 20 compounds from IBS (50,000 compounds) along with 68 anticancer compounds from published literature for GLIDE extra precision molecular docking. GLIDE-XP deliberated to figure out false-positives and furnish a better correlation between right poses and good scores. The foremost competent compounds have been selected for each target by optimal energy value, types of interactions, the potential for bonding, and conformations.

ADME properties studies

The majority of drug candidates don't succeed in clinical trials due to poor ADME properties. Therefore, in silico ADME/T (Absorption, Distribution, Metabolism, Excretion and Toxicity) predictive tools are cooperative strategy that could abolish indecorous compounds, before invested valuable time and money in primary testing of compounds. Computer based

Table 2 Lowest binding energy for the ligand-EGFR (PDB, 1 M17) protein interaction as detected by Maestro, version 9.6, Schrödinger. Our previous published article shows, myricetin (CID5281672) was recognized as dual-effective inhibitors for wild-Type EGFR and mutated EGFR (17)

Ligand type	Compounds ID	GScore	Lipophilic Evdw	HBond	Electro	Protein ligands interactions
EGFR Tyrosine Kinase Inhibitors (Control)	CID176870	−8.5	−5.36	−1.29	−0.27	Met 769 and Cys 773
	CID10184653	−8.5	−5.56	−1.25	−0.43	Met 769 and Cys 773
	CID208908	−7.1	−6.02	−0.66	−0.3	
	CID5328779	−6.94	−2.82	−2.29	−1.37	Asp831, Lys 721 and Met 769
	CID123631	−6.84	−5.49	−0.62	−0.17	Met 769
Anticancer Natural Compounds	CID5281672	−10.47	−3.49	−4.49	−1.42	Asp831, Lys 721 and Met 769
	CID5280343	−9.88	−3.32	−3.57	−1.88	Lys 721 and Met 769
	CID5280445	−9.25	−3.31	−3.42	−1.4	Asp831, Lys 721 and Met 769
	CID5280863	−8.98	−4.15	−2.55	−0.88	Glu 738 and Met 769
	CID65064	−8.59	−2.81	−5.51	−1.19	Cys 773, Lys 721 and Met 769
IBS	STOCK1N-80317	−12.18	−5.58	−4.27	−1.33	Met 769, Arg 817, and Asp 831
	STOCK1N-81095	−11.35	−4.47	−4.17	−1.85	Lys721, Met 769, Glu780, and Asp 831
	STOCK1N-36022	−9.28	−3.82	−2.48	−1.47	Met 769, Glu780, and Asp 831
	STOCK1N-56203	−9.26	−5.86	−1.6	−0.58	Met 769
	STOCK1N-41893	−9.14	−5.78	−1.06	−0.57	Met 769

Author's personal copy

Author's personal copy

Table 3 Lowest binding energy for the ligand-IR (PDB, 3ETA) protein interaction as detected by Maestro

Ligand type	Compounds ID	GScore	Lipophilic Evdw	HBond	Electro	Protein ligands interaction
IR,Tyrosine Kinase Inhibitors (Control)	CID24785538	−6.76	−4.75	−2.01	−0.76	Glu1047,Glu1077,Met1079,Phe1128, and Asp1150
	CID2044	−6.52	−4.61	−1.03	−0.28	Glu1077,Met1079, and Phe1151
	CID57390076	−5.42	−5.41	−0.72	−0.17	Hid1081, and Asp1083
	CID11353973	−4.4	−5.17	−1.03	−0.25	Phe1151, and Arg1155
	CID9825149	−3.29	−6.6	0	0.21	
Anticancer Natural Compounds	CID5281672	−9.92	−5.31	−3.29	−1.02	Leu1002,Met1079, and Phe1151
	CID9064	−9.16	−5.26	−2.85	−0.89	Leu1002,Met1079, and Phe1151
	CID56603750	−9.16	−7.23	−0.67	−0.93	Glu1047
	CID5281670	−9.1	−5.3	−2.87	−0.83	Leu1002,Met1079, and Glu1077
	CID65064	−8.94	−3.81	−4.28	−1.27	Arg1000, Met1079, and Asp1150
IBS	STOCK1N-67795	−10.34	−7.1	−0.98	−0.79	Glu1047, Met1079, and Phe1151
	STOCK1N-39395	−9.93	−7.11	−1.34	−0.83	Glu1047, Met1079, and Phe1151
	STOCK1N-73865	−9.86	−6.28	−0.98	−0.61	Glu1047 and Glu1077
	STOCK1N-70996	−9.84	−7.64	−1.57	−0.81	Glu1047, Met1079, and Asp1150
	STOCK1N-36722	−9.82	−7.07	−1.31	−0.87	Glu1047, Met1079, and Asp1150

theoretical approaches transpire to be the best option for prediction of ADME, for new compounds. Thus, ADME properties of best-docked compounds were predicted using QikProp application of Maestro 9.6. ADME/T properties are the prerequisite for the drug discovery and development process. Thus, these properties of selected best-docked ligands molecules were predicted. In silico, computational methods predict properties such as log BB, overall CNS activity, Caco-2 and MDCK cell permeability and logKhsa for human serum albumin binding, etc. [35, 36].

In vitro methodology

Chemicals

Myricetin was purchased from Sigma-Aldrich. Cell culture media, fetal bovine serum (FBS), trypsin, and 1 % penicillin and streptomycin were purchased from Invitrogen corporation and Ham's F-12K from Himedia.

Cell culture conditions and myricetin treatment

Cancer cell lines hepatocellular carcinoma (HepG2) and lung carcinoma (A549 and H460), and prostate cancer (PC3) was obtained from the NCCS, Pune (India). HepG2, A549, and H460 grown in phenol red DMEM media supplemented with 10 % heat-inactivated FBS, 1 % penicillin (100 units/ml), streptomycin (100 mg/ml). PC3 cells was grown in Ham's F-12K medium supplemented with 10 % FBS, 1 % penicillin (100 units/ml), streptomycin (100 mg/ml). All cells were maintained at 37 °C in a humidified atmosphere with 5 % CO2. Cells were exposed to different concentration of myricetin for 48 h. Cells incubated with culture medium with an equivalent amount of vehicle DMSO (final DMSO concentration was <0.2 %) served as controls.

Total RNA isolation, cDNA synthesis, and quantitative RT-PCR

One million cells/well were plated into the six well plates, culture media supplemented with 10 % FBS and 1 % penicillin/streptomycin and incubated at 37 °C. Cells were exposed to 80 μM myricetin for 48 h, and total RNA was extracted using Trizol (Life Technologies, Gaithersburg, MD) according to manufacturer's instructions. RNA quantified at 260/280 nm with thermo scientific nanodrop 2000 spectrophotometer and agarose gel electrophoresis. The absorption ratio A260 nm/A280 nm between 1.90 and 2 was taken into consideration for cDNA preparation. Approximately one microgram of total RNA was reverse-transcribed into cDNA using a high capacity PrimeScript 1st strand cDNA Synthesis Kit (Takara Bio Inc). mRNA expression was quantified by RT-PCR by using Veriti® 96-well fast

Author's personal copy

thermal cycler (Applied Biosystems). The following cycling parameters were optimized as follows: start at 95 °C for 5 min, denaturing at 95 °C for 30 s, annealing at 55 °C for 45 s, elongation at 72 °C for 45 s, and a final 5 min extra extension at the end of the reaction to ensure that all amplicons were completely extended and repeated for 40 amplification cycles [37]. GAPDH and β-actin used as a housekeeping gene to assure equal loading of the sample. Gel picture was taken by using automated image-capture and analyzed using system Gel Doc™ XR with Image Lab™ Software.

MTT assay

Cells viability was measured by a colorimetric assay composed of solutions of a tetrazolium compound MTT (dimethyl thiazolyl tetrazolium bromide). MTT produces a formazan product in a cell that is soluble in DMSO and recorded the absorbance of the formazan at 570 nm. Cells were seeded in to a 96 well plate at 7×10^3 cells per well supplemented with 10 % FBS, 1 % (*v/v*) penicillin/streptomycin and allowed to adhere overnight. After 24 h incubation, media was removed and FBS free media (serum starvation) was added. After treatment with the myricetin at various concentrations for 48 h, the medium was removed and washed with PBS and 100 µl of the MTT (0.5 mg/ml) was added to each well of the plate. Plates were incubated at 37 °C for 4 h, after incubation 100 µL of DMSO was added for solubilization of formazan and mix very well and was kept in the dark for 10 min. The intensity of the color developed was recorded at 570 nm in fluorescence microplate reader (Synergy /H1).

Determination of intracellular reactive oxygen species (ROS)

The conversion of non-fluorescent CM-H_2DCFDA to fluorescent DCF was used to measure the intracellular production of ROS. Cells were seeded in a 96 well plate at 7×10^3 cells per

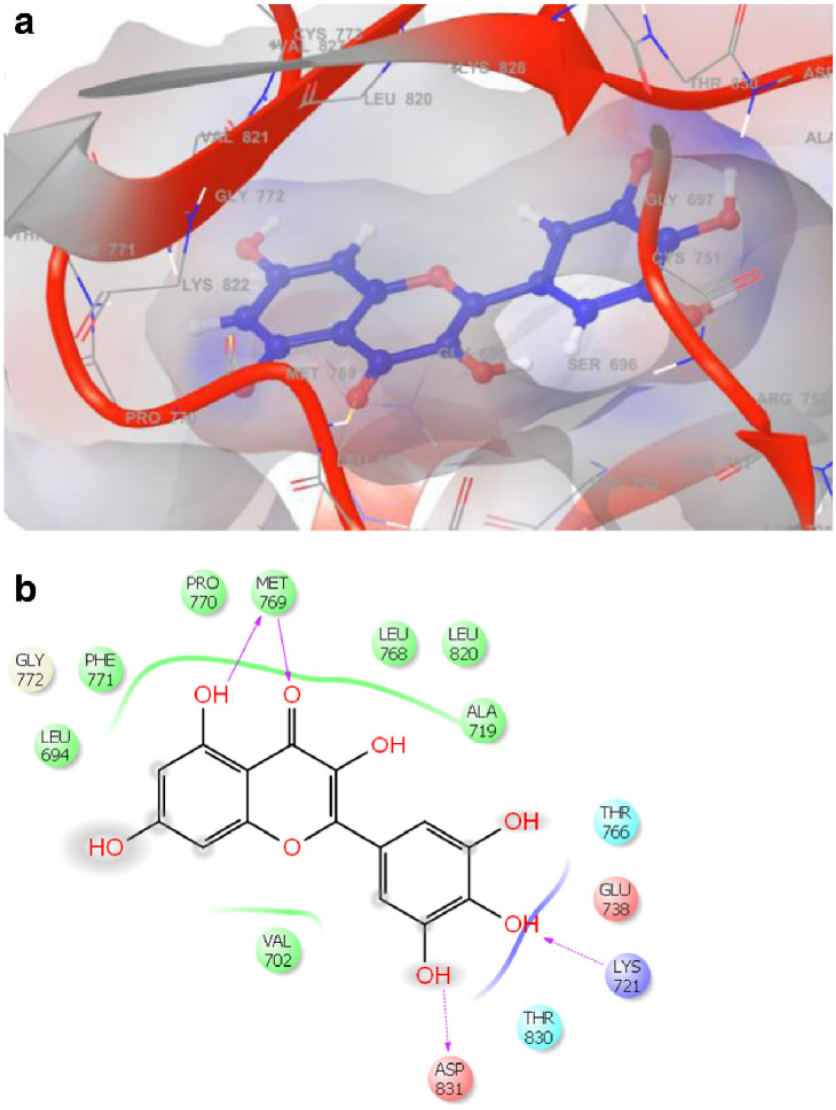

Fig. 2 **a** Ribbon presentation of EGFR (PDB; 1M17) with CID5281672 (myricetin). **b** Protein-ligand interactions profile of 1M17 with myricetin

Author's personal copy

well supplemented with 10 % FBS, 1 % penicillin/streptomycin and allowed to adhere overnight. Treatment with myricetin at various concentrations for 48 h, the medium was removed and washed with PBS and 100 µl of the CM-H_2DCFDA (5 µM) was added to each well of the plate. Plates were placed in an incubator for 4 h, and the fluorescence intensity was measured with excitation at 485 nm and emission at 530 nm using a fluorescence microplate reader (Synergy /H1).

Cell migration assay (In vitro wound-healing assay)

Cell migration procedure adapted from previous publish article [19, 38]. One million cells were seeded in a six-well plate and grown overnight and allowed to adhere. Next day, cultures were replaced with fresh medium containing 0.5 % FBS medium (Serum starvation). Cells were treated with different concentration of myricetin; monolayer cells were scratched with a 200 µl pipette tip to create a wound and wash with

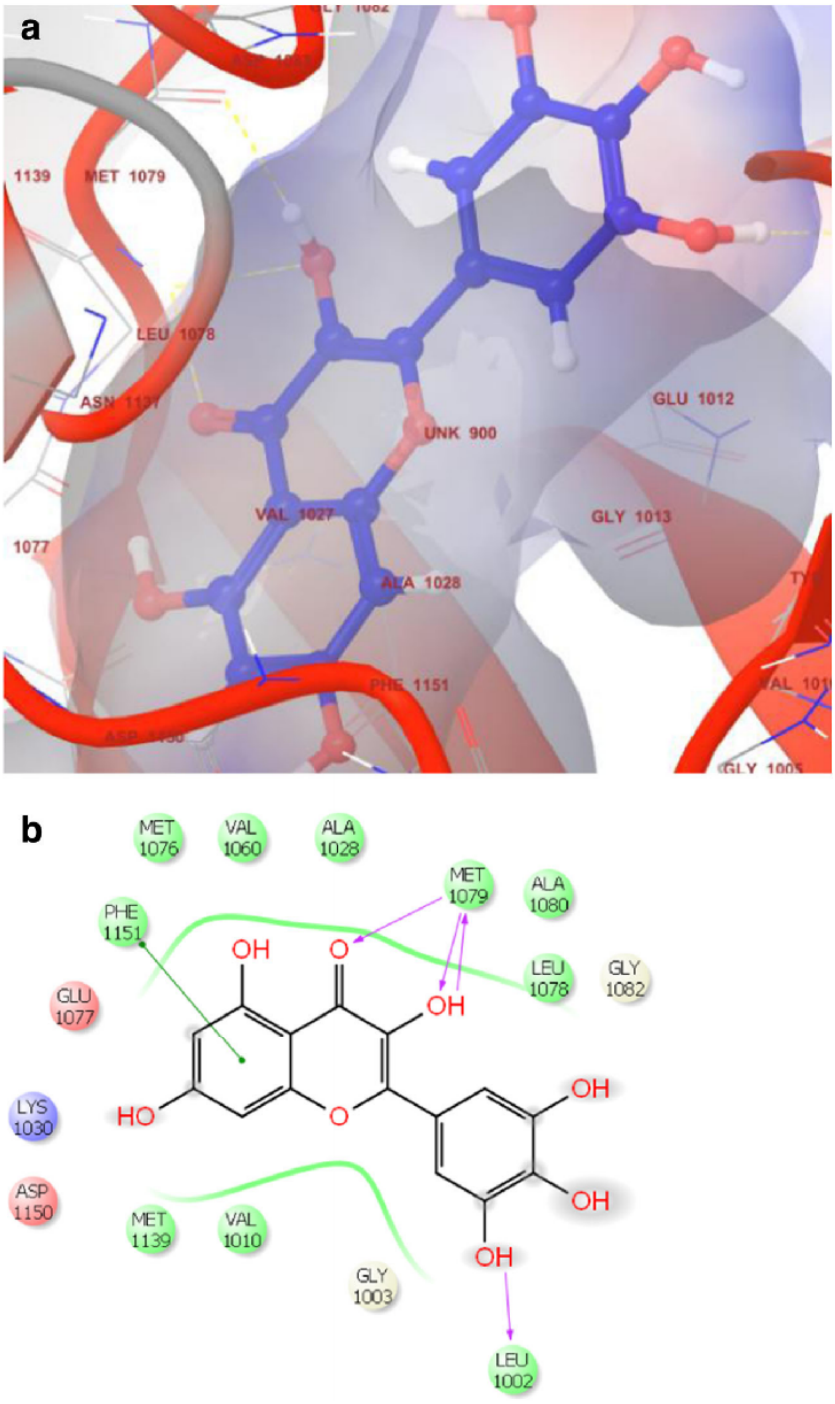

Fig. 3 **a** Ribbon presentation of IR (PDB, 3ETA) with CID5281672 (myricetin). **b** Protein-ligand interactions profile of 3ETA with myricetin

Table 4 Evaluation of drug-like properties of the lead molecules by Qikprop Maestro

Compounds	QP log $P_{o/w}$ (−2.0 to 6.5)	QPlog HERG (acceptable range: above −5.0)	QPP Caco (nm/sec) <25-poor >500- great	QP log BB (−3-1.2)	QPP MDCK (nm/sec) <25-poor >500- great	QPlog Kp (−8.0 to −0.1)	QPlog Khsa (Acceptable range: −1.5 to 1.5).	Percentage of human oral absorption; (<25 % is poor and >80 % is high)
CID9064	0.481	−4.737	53.349	−1.875	20.822	−4.707	−0.41	60.671
CID65064	−0.243	−5.716	1.018	−4.333	0.288	−7.513	−0.439	0
CID72277	−0.17	−4.577	20.038	−2.345	7.225	−5.575	−0.546	36.292
CID457964	1.916	−3.138	351.773	−1.054	159.924	−3.761	−0.001	83.738
CID5280343	0.522	−5.356	21.055	−2.418	7.623	−5.353	−0.316	53.688
CID5280445	0.96	−5.051	42.097	−1.946	16.119	−4.851	−0.19	61.636
CID5280863	1.059	−5.079	58.254	−1.802	22.899	−4.534	−0.196	64.74
CID5281670	0.41	−4.927	23.361	−2.244	8.529	−5.329	−0.35	53.842
CID5281672	−0.281	−4.869	7.525	−2.827	2.507	−6.323	−0.491	28.028
CID56603750	2.644	−7.882	4.196	−5.099	1.333	−8.512	−0.172	14.699
STOCK1N-81095	2.083	−3.888	0.67	−4.068	0.234	−6.435	−0.129	0
STOCK1N-36022	1.138	0.97	0.174	−2.417	0.088	−6.266	−0.962	20.015
STOCK1N-56203	3.225	−5.92	721.644	−0.839	347.707	−1.776	0.052	96.989
STOCK1N-41893	4.293	−5.655	1392.899	−0.736	707.799	−1.536	0.543	100
STOCK1N-67795	5.314	−7.425	1439.362	−0.897	733.353	−1.073	0.806	88.67
STOCK1N-39395	4.461	−6.965	835.175	−0.713	1249.845	−1.559	0.525	100
STOCK1N-73865	4.535	−6.95	823.428	−0.965	401.006	−1.687	0.762	100
STOCK1N-70996	3.516	−7.056	378.595	−1.468	173.144	−2.071	0.299	93.676
STOCK1N-36722	4.248	−7.061	852.852	−0.794	754.083	−1.424	0.484	100

QPlogPo/w (−2.0 to 6.5) Predicted octanol/water partition coefficient

QPlogHerg (acceptable range: above −5.0) Predicted IC50 value for blockage of HERG K+ channels;

QPPCaco (nm/sec) <25-poor >500- great Predicted apparent Caco-2 cell permeability in nm/sec. Caco-2 cells is a model for the gut blood barrier,

QPlogBB (−3−1.2) Predicted brain/blood partition coefficient;

QPPMDCK (nm/sec) <25-poor >500- great Predicted apparent MDCK cell permeability in nm/sec. MDCK cells are considered to be a good mimic for the blood–brain barrier

QPlogKP- Predicted skin permeability; Q P log Khsa-

Prediction of binding to human serum albumin; (acceptable range: −1.5 to 1.5)

Percentage of human oral absorption; (<25 % is poor and >80 % is high)

Author's personal copy

Author's personal copy

media to removed floating cells and incubated for 48 h. The rate of wound closure was analyzes and photographed after 48 h and adding scale bars to images using ImageJ.

Statistical analysis

Statistical analysis was done using SigmaPlot 11. Statistical values are expressed as the mean±SEM. Data was analyzed using Kruskal-Wallis one-way analysis of variance on ranks followed by followed by Tukey statistical analysis. The value of $p<0.05$ was considered statistically significant.

Results and discussions

Molecular docking of compounds with EGFR, IR, IGF1R, VEGFR1, and VEGFR2

Overexpression or overactivity of RTKs such as EGFR, IR, IGF1R, and VEGF receptor has been well known in a variegated cancer cells, including prostate, breast, lung and ovarian cancers. Recently, we performed multitargeted molecular docking of EGFR, IR, IGF1R, and VEGFR against natural compounds. The lowest energy conformation, representing the best binding structure of inhibitors to receptor, was identified by the molecular docking procedure. The protein-ligands interactions yielded a cornucopia of information highlighting the irrefutable role portrayed by numerous factors namely hydrogen bonds, salt bridges, metal interactions, lipophilic interactions, π-π and π-cation interactions in the protein-ligand interactions profile. The data obtained from molecular docking various parameter including their Gscore, hydrogen bond, electrostatic bond, and amino acid residues are illustrated in Tables 2 and 3. In the present study, CID5281672 (myricetin) showing high Gscore for EGFR and IR as compared to respective control. Molecular docking result of EGFR (PDB, 1M17) and IR (PDB, 3ETA) against natural compounds revealed that myricetin have better Gscore −10.47 and −9.92 Kcal/mol respectively. The crystal structure of the 1M17 and 3ETA has been determined with 2.6-Å resolution. Protein-ligands interactions revealed that amino acid Leu694, Leu768, Met769, Pro770, Phe771, and Leu820 of 1M17 involve in the hydrophobic interactions with the myricetin. In addition, amino acid Lys721 and Asp831, involved in sidechain hydrogen bond and Met769 amino acid included in back-bone hydrogen bond at the active site of 1M17. Moreover, protein-ligand interactions of 3ETA with the myricetin showed that Val1010, Ala1028, Val1060, Met1076, Leu1078, Met1079, Ala1080, and Phe1151 involve in the hydrophobic interactions with the myricetin. Additionally, Leu1002 and Met1076 amino acid included in back-bone hydrogen bond at the active site of 3ETA with the myricetin. Moreover, amino acids Phe1151 of 3ETA form pi-pi stacking interaction in the active site of 3ETA. Moreover, molecular docking result of 1M17 against natural compounds revealed compound CID5280343, CID5280445, CID5280863, CID65064, STOCK1N-80317, STOCK1N-81095, STOCK1N-36022, STOCK1N-56203, and STOCK1N-41893 have better Gscore (as compared to control) -9.88, −9.25, −8.98, −8.59, −12.18, −11.35, −9.28, −9.26, and −9.14 Kcal/mol respectively. Furthermore, compounds CID9064, CID56603750, CID5281670, CID65064, STOCK1N-67795, STOCK1N-39395, STOCK1N-73865, STOCK1N-70996, and STOCK1N-36722 have Gscore −9.16, −9.16, −9.1, −8.94, −10.34, −9.93, −9.86, −9.84, and −9.82 Kcal/mol respectively when docked with 3ETA (Figs. 2 and 3).

ADME/T studies

ADME/T (absorption, distribution, metabolism, elimination and toxicity,) properties of myricetin were assessed through the Qikprop application of Maestro 9.6. Myricetin was found to be encouraging based on their docking free energy score (Gscore) and ADME/T properties. Most interesting aspect of myricetin is their excellent QPlogPo/w, QPlogHerg K^+

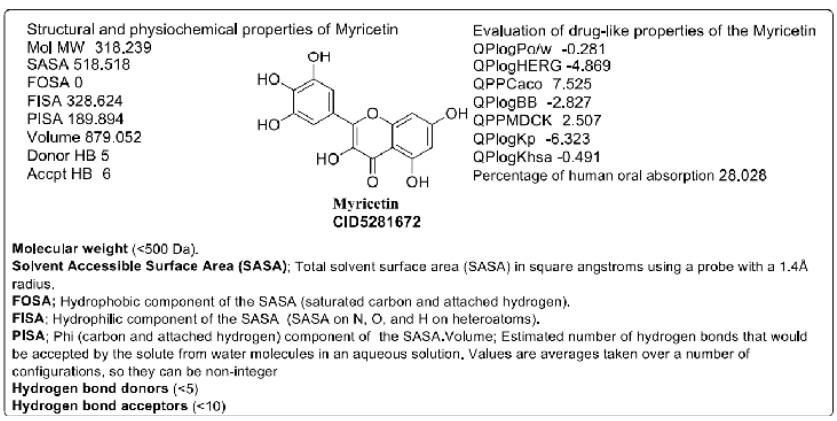

Fig. 4 ADME/T properties. Structural, physicochemical, biochemical, pharmacokinetics and toxicity properties of myricetin were appraised by using the Qikprop application of Maestro 9.6

Author's personal copy

channels, QPlogBB, QPlogKP, QPlogKhsa values that fulfill the Lipinski's rule of five (Table 4 and Fig. 4). However, these compounds do not have very good QPP Caco, QPP MDCK values and percentage of human oral absorption. Therefore, myricetin structural modifications and optimization are required to predict structures that have better QPP Caco, QPP MDCK and percentage of human oral absorption activity. IBS compounds STOCK1N-41893, STOCK1N-39395, STOCK1N-73865, STOCK1N-36722, and STOCK1N-08688 have 100 % percentage of human oral absorption and other value such as QPlogPo/w, QPlogHerg K^+ channels; QPlogBB, QPlogKP, QplogKhsa, QPPCaco, and QPPM DCK fulfill the Lipinski's rule of five. These compounds may be used to further for biological evaluation as an RTKs inhibitor.

Effect of myricetin on EGFR, mTOR, Bid, Bcl-2, and IR mRNA expression in cancer cell lines

The mRNA expression of total IR isoform, EGFR, mTOR, Bid, and Bcl-2 was determined using the RT-PCR analysis. One band for each mRNA studied was observed at the estimated size to determine the specificity of each primer set. We investigated whether myricetin could impede EGFR, IR, mTOR, Bid, and Bcl-2 expression in HepG2, A549, H460, and PC3 cells. Cells were incubated for 48 h with the myricetin and determine the mRNA expression by using RT-PCR. Interestingly, RT-PCR results show that the myricetin have a potential for robust inhibition of EGFR and mTOR mRNA expression. Furthermore, pro-apoptotic proteins Bid and anti-apoptosis protein (Bcl-2) expression was determined by RTPCR. Moreover, myricetin reduces the Bcl2 expression and induce the pro-apoptotic proteins Bid expression. The RT-PCR densitometric bands analysis showed that myricetin reduced the mRNA expression of EGFR by 20, 30, 50, and 20 % in HepG2, A549, H460, and PC3 cells respectively at 80 μM concentration. Meanwhile, myricetin diminished the mRNA expression of IRA by 35, 50, and 35 % in HepG2, A549, and H460, and at the same time myricetin reduced the mRNA expression of IRB by 40 and 30 % in HepG2 and A549 respectively. Moreover, myricetin decreased the mRNA expression of mTOR by 50, 20, 10, and 26 % in HepG2, A549, H460, and PC3. Myricetin increased the mRNA expression of Bid by 45 and 50 % in H460 and PC3 at 80 μM concentration. As long as, myricetin decreased the mRNA expression of bcl-2 by 50, 20, 10, and 26 % in HepG2, A549, H460, and PC3 (Fig. 5). The primer Sequences used in the study listed in Table 5.

Effects of myricetin on cell growth of cancer cells

To evaluate the cytotoxicity of myricetin in cancer cell lines, MTT assay was performed. Cells were cultured with 5, 10, 20, 40, and 80 μM myricetin for 48 h. Myricetin exhibited a remarkable reduction of cell proliferation against cancer cell lines in a concentration-dependent manner at concentrations between 5 and 80 μM. Furthermore, myricetin evinces a reduction of cell proliferation against lung cancer cells A549 in a concentration-dependent manner. The mean 30 % inhibitory concentration of myricetin on cell growth was at

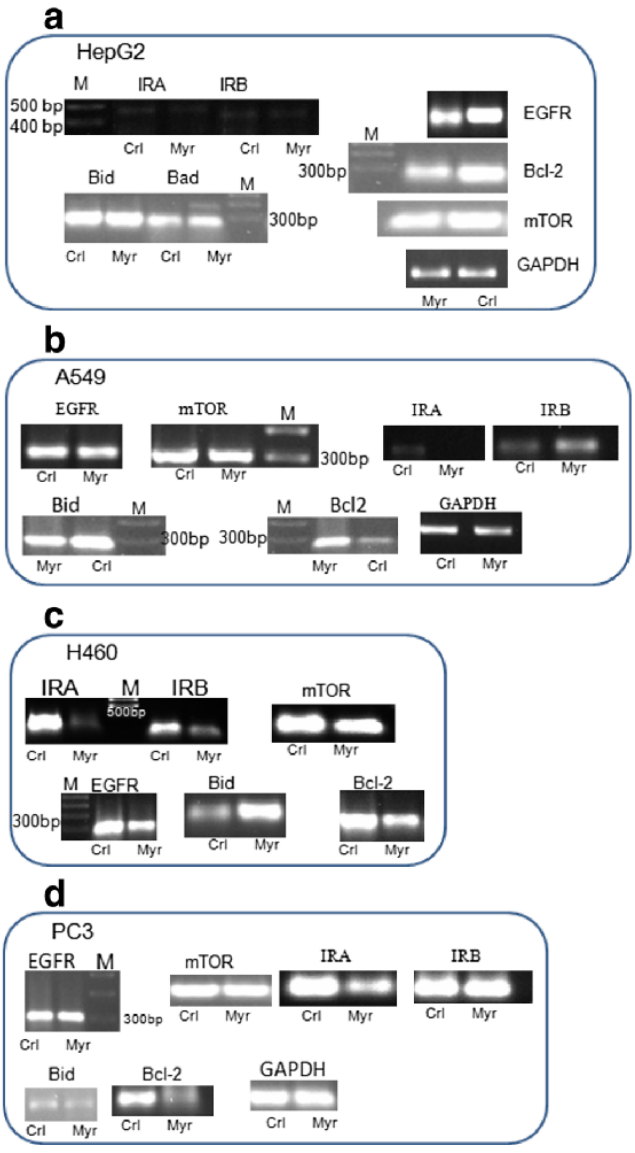

Fig. 5 Effect of myricetin on IR, EGFR, mTOR, Bid and Bcl2 mRNA turnover in selected four cells (**a**, **b**, **c**, and **d**). Cells were treated with 80 μM myricetin for the indicated time periods. IR, EGFR, mTOR, Bid and Bcl2 mRNA levels were determined by RT-PCR and normalized to β-actin and GAPDH as the loading control. mRNA of IR, EGFR, mTOR, Bid, and Bcl2 has changed in cells treated with myricetin treatment (**e**, **f**, **g**, **h**, **i**, and **j**). Myricetin down-regulated the expression of IR, EGFR, and mTOR. Moreover, myricetin inhibited the mRNA expression of anti-apoptotic gene products Bcl-2 but up-regulated the expression of apoptotic gene product Bid. [Crl (Control), Myr (myricetin)]

Author's personal copy

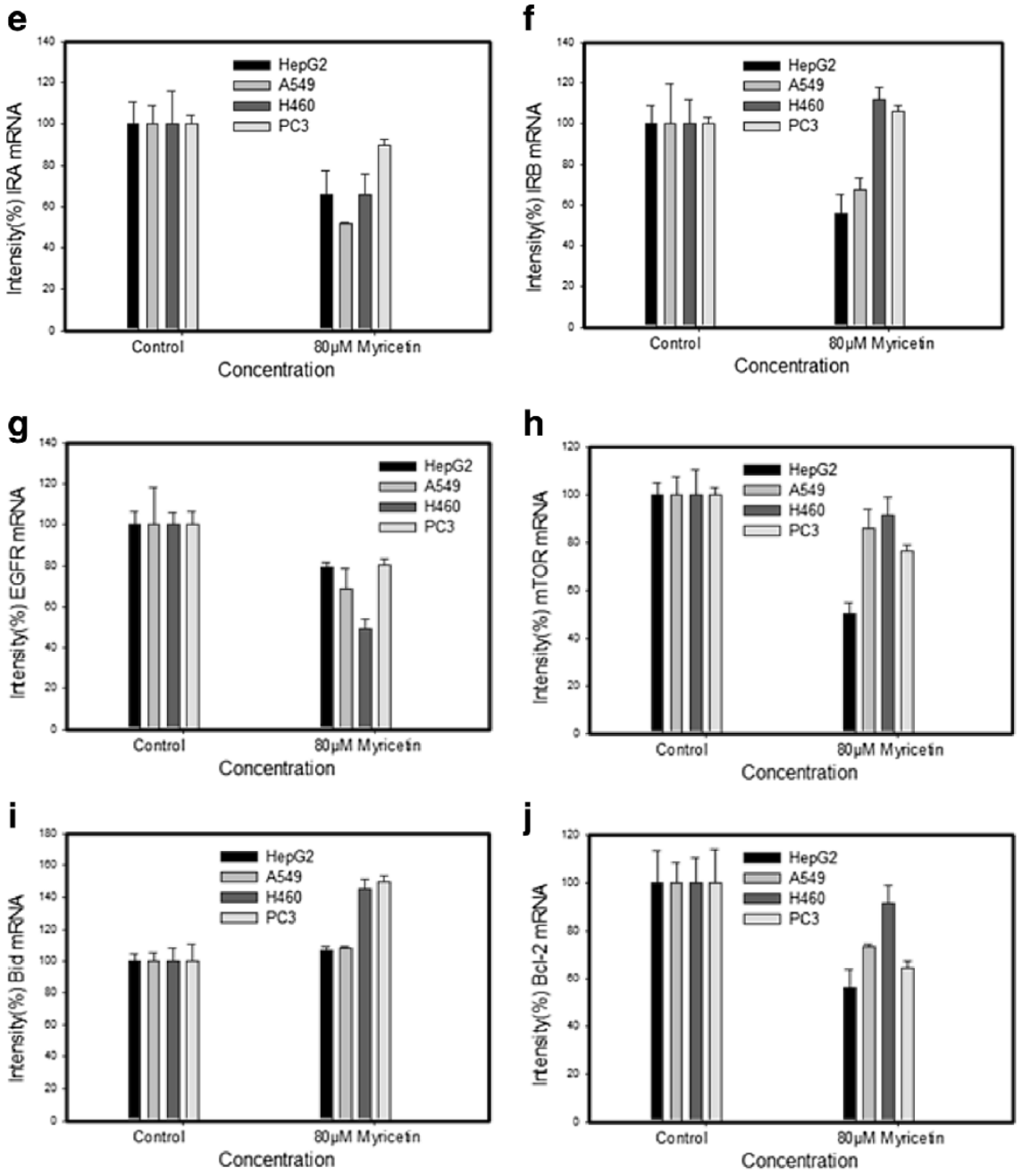

Fig. 5 (continued)

20 μM on A549 cells for 48 h treatment (**$P < 0.01$). While, the mean 50 % inhibitory concentration of myricetin on cell growth was at 80 μM in PC3 cells (***$P < 0.001$). Our previously published literature showed that myricetin treatment on HepG2 and H460 cells reduces the cell proliferation [22]. A number of reports confirm that the myricetin execute a critical role in the inhibition of PC3 cell apoptosis in a dose-dependent manner. Although, a noticeable synergistic effect on inhibition of cell proliferation was observed when myricetin was used in combination with myricitrin, Myricetin alone was also equally adept in inhibiting the cell proliferation of HL-60 (leukemia), HepG2 (hepatoma), pancreatic Cancer (MIA PaCa-2, Panc-1and S2-013) and T24 cells in a dose and time-dependent manner [19, 20, 18]. Moreover, Myricetin was found to impede H2O2-induced apoptosis in Chinese hamster lung fibroblast (V79-4) cells (Fig. 6a).

Author's personal copy

Myricetin reduces ROS level in cancer cells

The conversion of non-fluorescent CM-H2DCFDA to fluorescent DCF was used to measure the intracellular production of ROS. Myricetin exposures, significantly reduces the ROS generation, were observed on HepG2, A549, H460, and PC3 cells after 48 h treatments. Cells were cultured with 5, 10, 20, 40, and 80 μM myricetin for 48 h and calculated the ROS reduction. The mean 40 % ROS reduction at 40 μM on A549 cells (***$P<0.001$), whereas, 30 % ROS reduction at 80 μM concentration in HepG2 (***$P<0.05$) and PC3 (***$P<0.001$) cells. Furthermore, in-vivo, treatment of myricetin on orthotropic pancreatic tumors, increases the tumor regression and decreased metastatic spread. Myricetin-induced apoptosis by modulating the PI3K and p38 MAPK signaling pathways on human T24 bladder cancer cells and HepG2 Cells [19, 20] (Fig. 6b).

Cell migration assay

We investigate whether the treatment of myricetin inhibits the migration of HepG2, A549, H460, and PC3 cells. For instance, we determine the effect of concentrations 5 to 80 μM of myricetin on HepG2, A549, H460, and PC3 cells. Representative photomicrographs of the HepG2 and PC3 cells after the treatment of different concentration of myricetin shown in Fig. 7(a, c). Figure 7(b, d) showed the migration of HepG2 and PC3 cells treated with different concentrations of myricetin relative to untreated control cells. Treatment with the myricetin (5, 10, 20, 40 and 80 μM) reduced the migration of selected cells and increases the wound in a concentration-dependent manner. The mean 50 % increases the wound at 80 μM on PC3 (**$P<0.01$) cells.

Myricetin was observed to ameliorate inoperative insulin signaling via β-endorphin signaling in the skeletal muscles of fructose-fed rats. Myricetin enhances the secretion of β-endorphin, followed by peripheral μ-opioid receptors activation which leads to amelioration of impaired insulin receptors signaling [39, 40]. JAK1/STAT3 pathway in its role as a second

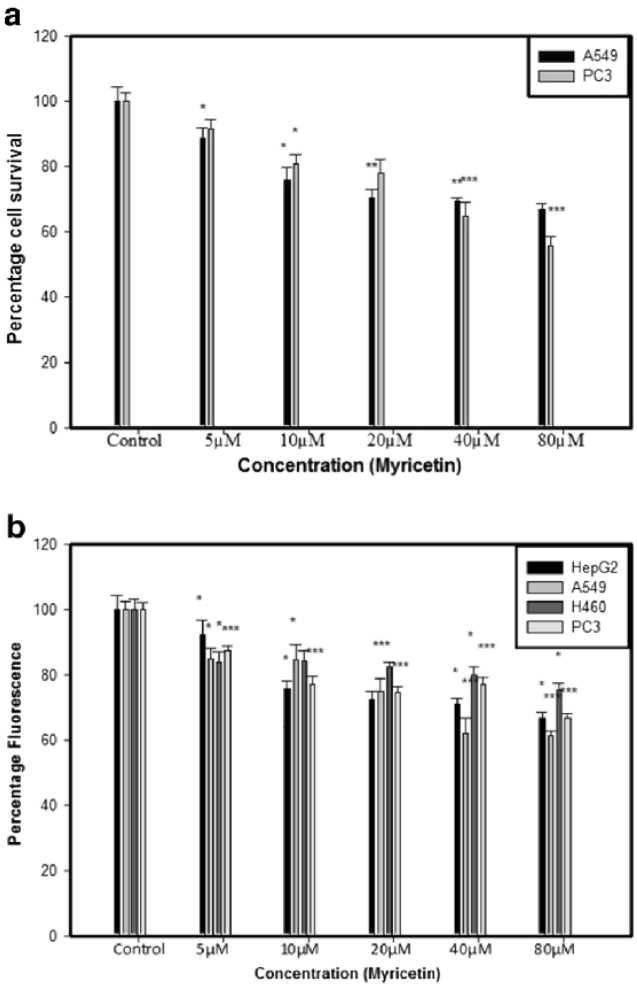

Fig. 6 **a** Affect of myricetin on the cell growth in A549 and PC3 cells after the treatment of 5, 10, 20, 40, and 80 μM myricetin for 48 h. Myricetin reduces the cell growth of the A549 and PC3 cells in a dose-dependent manner determined by the MTT assay. **b** Affect of myricetin on oxidative stress in HepG2, A549, H460, and PC3 cells. Myricetin reduces ROS level on the HepG2, A549, H460, and PC3 cells in a dose-dependent manner determined by the CM-H_2DCFDA fluorescent based assay. *$P<0.05$, **$P<0.01$, and ***$P<0.001$ versus controls

Table 5 Primer sets used for amplification

Sr. No.	Name of gene	Forward primer (5′ to 3′)	Reverse primer (5′ to 3′)
1	IR-A	TGAGGATTACCTGCACAACG	ACCGTCACATTCCCAACATC
2	IR-B	CGTCCCCAGAAAAACCTCTTC	GGACCTGCGTTTCCGAGAT
3	mTOR	CCAACAGTTCACCCTCAGGT	GCTGCCACTCTCCAAGTTTC
4	Bcl-2	CATGTGTGTGGAGAGCGTCAA	GCCGGTTCAGGTACTCAGT CA
5	Bid,	GCTGTATAGCTGCTTCCAGTGTA	GCTATCTTCCAGCCTGTCTTCTC
6	EGFR	5′ATGCCCGCATTAGCTCTTAG3′	5′GCAACTTCCCAAAATGTGCC3′
7	β-Actin	GTGGGGCGCCCCAGGCACCA	CTCCTTAAGTCACGCACGATTTC
8	GAPDH	ACGGATTTGGTCGTATTGGGCG	CTCCTGGAAGATGGTGATGG

Author's personal copy

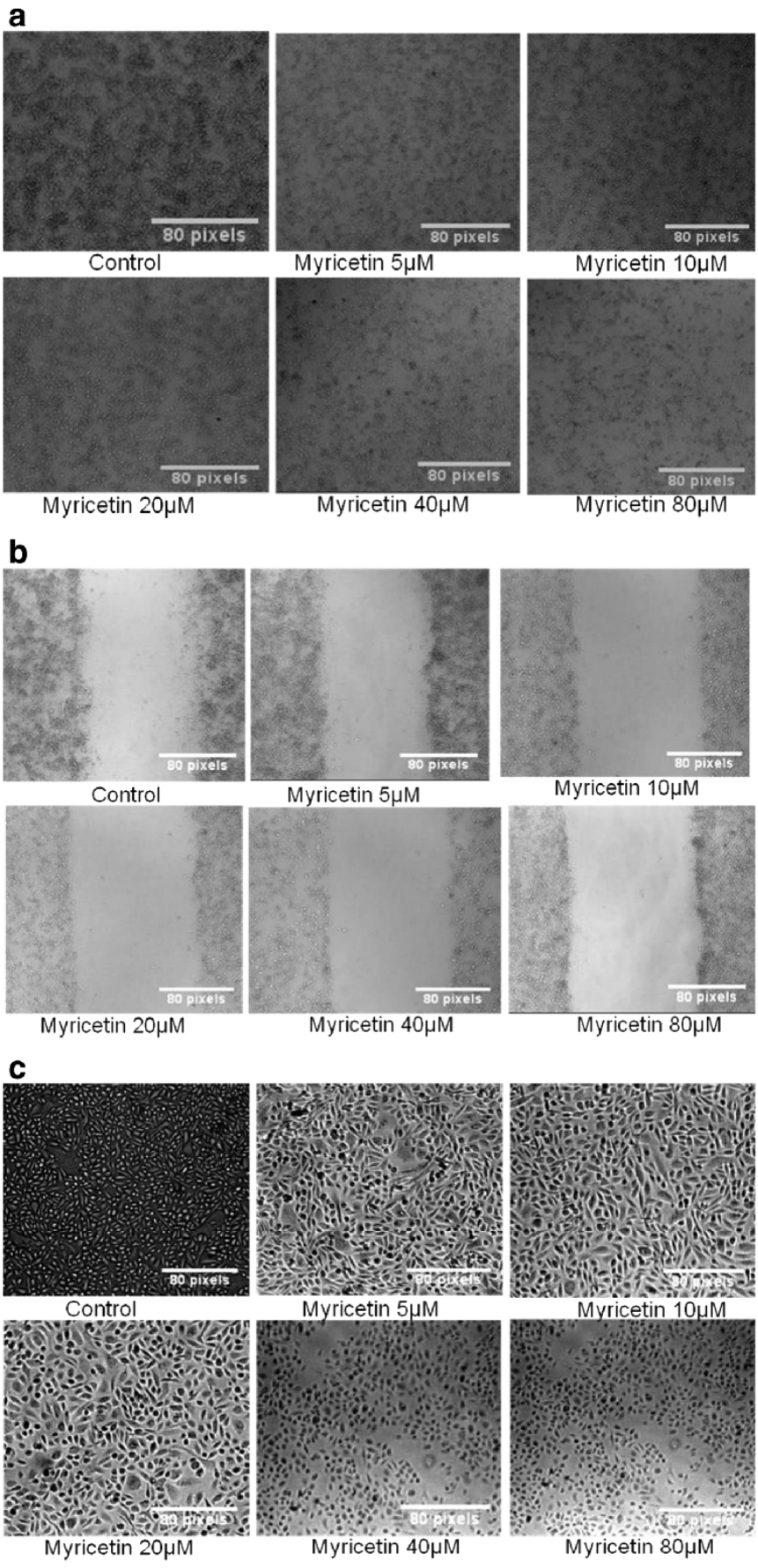

Author's personal copy

◀ **Fig. 7** Myricetin reduces cell migration in the HepG2, A549, H460, and PC3 cells determined by wound-healing assay. Representative photomicrographs of the HepG2 and PC3 cells after the treatment of different concentration of myricetin (**a** and **c**). One million HepG2 and PC3 cells were seeded in a six-well plate and grown overnight and allowed to adhere overnight. Next day, cultures were replaced with fresh medium containing 0.5 % FBS medium (Serum starvation). Cells were treated with different concentration of myricetin; monolayer cells were scratched with a 200 μl pipette tip to create a wound and wash with media to removed floating cells and incubated for 48 h. The rate of wound closure was analyzes and photographed after 48 h and adding scale bars to images using ImageJ (**b** and **d**). Figure **e** shows that width of wound increases after the treatment of myricetin for 48 h in all selected cell lines. *$P<0.05$, **$P<0.01$, and ***$P<0.001$ versus controls

messenger is a well-known cell signaling cascade involved in regulating numerously cellular processes, viz. Growth, development and maintenance of immune system homeostasis. JAK1/STAT3 pathway activated by cytokine and growth factor including insulin; IGF1 and EGF have been advocating a significant role in cell proliferation [41, 42]. It is reported that myricetin, bind to JAK1/STAT3 to inhibit cell transformation in EGF activated mouse JB6P^{+} cells [43].

A number of reports, confirm that myricetin inhibiting the cell proliferation of leukemia (HL-60), hepatoma (HepG2), prostate cancer (PC3) and urinary bladder carcinoma (T24) cells in a dose and time-dependent manner [19, 44, 20]. Moreover, myricetin was also found to inhibit H_2O_2 induced apoptosis in Chinese hamster lung fibroblast (V79-4) cells. As evident in several reports, flavonoid myricetin induced apoptosis and cell cycle arrest followed by inhibiting cell proliferation via decreasing the activity of PI3K pathways in primary and metastatic pancreatic cancer cells. It is evidenced that, myricetin could directly target Akt serine/threonine kinase to inhibit cell transformation via competing with ATP [45, 46]. Myricetin was seen to induce apoptosis by modulating the metabolic PI3K and mitogenic MAPK

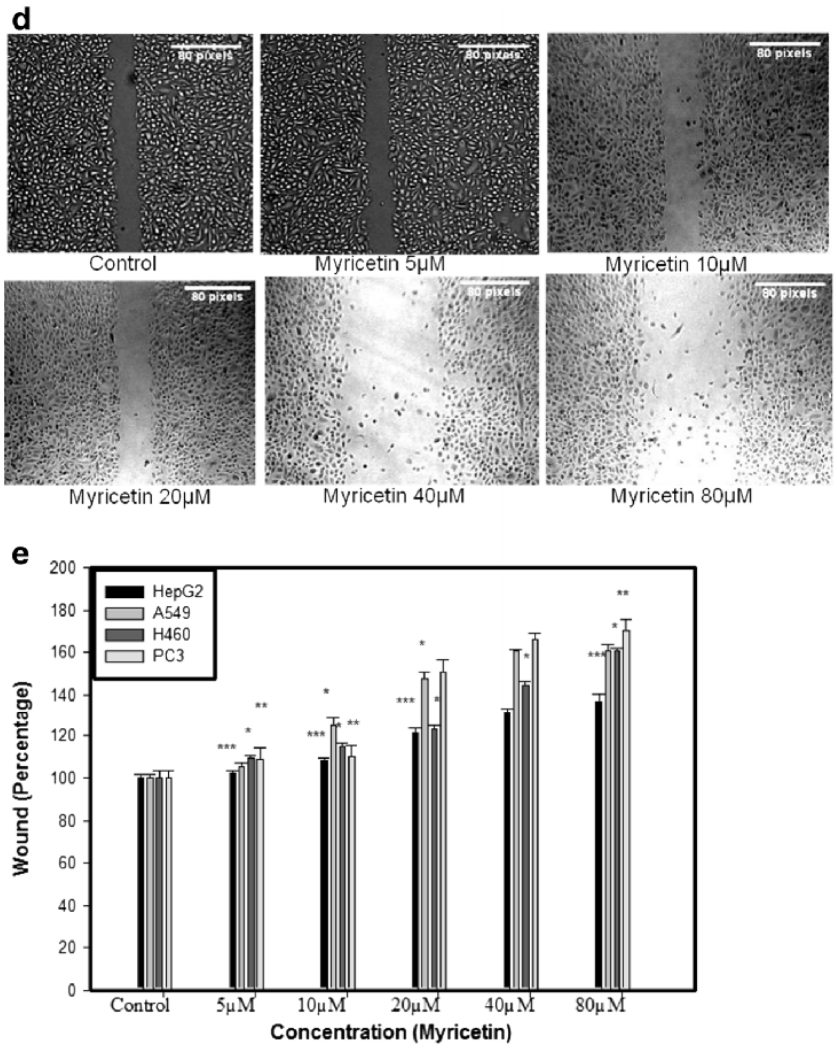

Fig. 7 (continued)

Author's personal copy

signaling pathways in hepatoma, urinary bladder carcinoma, prostate cancer, and skin cancer cells [47, 48]. Myricetin has been shown to restrain the cell proliferation of hepatoma and oesophageal adenocarcinoma cells via inducing G2/M phase arrest [49–51].

Molecular docking of compounds with androgen receptors (AR) and estrogen receptors (ER)

The AR and ER are expressed in many tissues and has been found to play an important roles in hormone-dependent tumorigenesis and metastasis in number of cancers such as prostate, bladder, kidney, lung, breast and liver [52, 53]. In this context, we performed molecular docking study of AR against selected natural compounds. Molecular docking results indicate that the myricetin have better Gscore then previously available drugs such as bicalutamide and nilutamide. Molecular docking results of 2PIV against selected natural compounds disclosed that the myricetin have better Gscore −10.47 Kcal/mol respectively. Moreover, protein-ligand interactions of 2PIV with the myricetin divulge that Leu704, Leu 707, Trp741, Met742, Val746, Met749, Met780, Leu873, and Phe876 involve in the hydrophobic interactions. Furthermore, Asn705 amino acid included in sidechain hydrogen bond, and Thr877 amino acid included in back-bone hydrogen bond at the active site of AR with myricetin. Moreover, amino acids Phe764 of AR form pi-pi stacking interaction in the active site of AR. Molecular docking results of 3ERT against selected natural compounds disclosed that the myricetin have Gscore −7.7 Kcal/mol and protein-ligand interactions same as an anti-ER compounds CID449459 (Afimoxifene) and CID104741 (Fulvestrant). Amino acids Met343, Leu347, Trp383, Leu384, Tyr526, and Met528 involve in the hydrophobic interactions. Amino acid Asp351 and Leu525 intricate in sidechain hydrogen bond and backbone hydrogen bond interactions respectively with myricetin (Fig. 8, Tables 6 and 7). Moreover, cross-talk with growth factor at downstream signaling led to the emergence of androgen-independent prostate tumors. It is reported that wine-derived phenolics compounds piceatannol and myricetin act as agonists for ERα in breast cancer cells [54]. AR and receptor RTKs cross-talk at the downstream level leads to increases tissue-specific cell proliferation [55–59]. Flavonoids exhibit antitumor activity in AR-positive as well as AR-negative prostate cancer cell lines whereas in the case of breast cancer ER¯positive and negative cell lines. Consequently, it was reported that flavonol aglycones (quercetin, fisetin, galangin, kaempferol, and myricetin) exert enough intense cytotoxic activity on AR-dependent

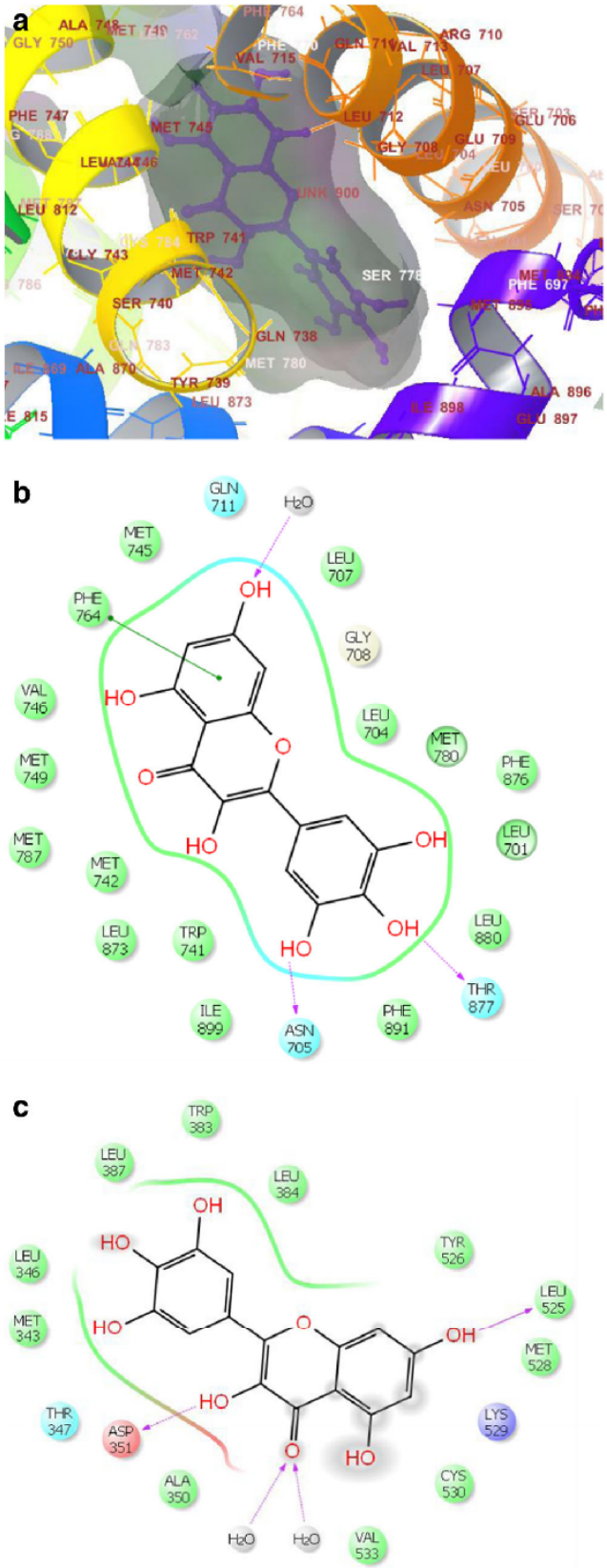

Fig. 8 **a** Ribbon presentation of AR (PDB, 2PIV) with CID5281672 (myricetin). **b** Protein-ligand interactions profile of 3ETA with myricetin. **c** Protein-ligand interactions profile of 3ERT with myricetin

Author's personal copy

Table 6 Lowest binding energy for the ligand-AR (PDB, 2PIV) protein interactions as detected by Maestro

Ligand type	Compounds ID	GScore	Lipophilic Evdw	HBond	Electro	Protein-ligands interaction
AR Inhibitors (Control)	CID2375	−5.87	−5.87	−0.85	0	Asn705, Phe764, and Thr 877
	CID4493	−5.37	−4.14	−0.36	−0.21	Asn705, Phe764, and Thr 877
Anticancer Natural Compounds	CID5281672	−10.05	−4.67	−3.83	−0.99	Asn705, Phe764, and Thr 877
	CID65064	−9.95	−5.4	−4.26	−1.54	Leu701,Asn705, Phe764, and Thr 877
	CID72277	−9.45	−4.81	−2.99	−0.96	Asn705, Phe764, and Thr 877
	CID5280343	−9.3	−4.59	−3.4	−0.66	Asn705, Phe764, and Thr 877
	CID457964	−9.15	−4.81	−2.88	−0.97	Asn705, and Thr 877
IBS	STOCK1N-53104	−10.21	−5.79	−2.33	−1.03	Asn705, and Arg752
	STOCK1N-26380	−9.73	−5.6	−1.59	−0.95	Asn705, Arg752, and Thr 877
	STOCK1N-21131	−9.4	−5.77	−1.51	−0.89	Asn705, and Arg752
	STOCK1N-08688	−9.08	−5.73	−1.35	−0.8	Asn705, and Met745
	STOCK1N-53196	−9.02	−5.69	−1.38	−0.43	Leu701, and Arg752

Table 7 Lowest binding energy for the ligand-ER (PDB, 3ERT) protein interactions as detected by Maestro

Ligand type	Compounds ID	GScore	Lipophilic Evdw	HBond	Electro	Protein-ligands interactions
ER inhibitors (Control)	CID449459	−10.4	−7.04	−0.87	−1.02	Glu353 and Arg394
	CID104741	−9.72	−5.82	−0.79	−0.99	Glu353 and Arg394
	CID5281672	−7.77	−2.8	−3.81	−1.02	Asp351 and Leu525

prostate cancer cells [60]. Furthermore, it was observed that the flavonols quercetin, kaempferol, and myricetin inhibited hepatocyte growth factor signaling in a medulloblastoma cell line, that led to the inhibition of cell migration [61]. More work is required in the AR sensitive LNCaP prostatic cell line and ER^+ breast cancer cells to ascertain biological effect of myricetin on AR/ER.

Conclusion

The results of the present study demonstrate that, docking free energy calculated the excellent dock score for the myricetin when docked with EGFR, IR, and AR\ER. Information acquire from these studies can prove to be useful to fathom the protein-ligand interactions that are required to strengthen the cell growth inhibitory activity, as well as ADME/T properties. MTT results indicate that the myricetin inhibit the cell viability and proliferation of cancer cells in a dose-dependent manner. Treatment of myricetin in cancer cell lines led to down-regulation of mRNA expression of EGFR, IR, mTOR, and Bcl-2. Collectively, these results indicate that the myricetin reduces cell proliferation of cancer cell through EGFR and IR followed by mTOR signaling. Our in silico and in vitro data compiled from the current study cannot only be usefulness in myricetin anticancer activity, but also in the medley of bioactive basic skeleton (parent compounds) to design and synthesize novel potent anticancer compounds. Structural modification of the natural myricetin skeleton may be help to improved anticancer activity as well as ADME/T properties. Although, further in vitro and in vivo experimental studies are needed for the experimental validation of our findings.

Acknowledgments We would like to thank Vice Chancellor, Central University of Punjab, Bathinda, Punjab, (India) for supporting this study with infrastructural requirements. We also thank Professor P. Ramarao (Dean, Academic Affairs) Central University of Punjab, Bathinda, Punjab, India for his suggestions during the course that tremendously helped to improve this article. This study was also supported by a Senior Research Fellowship grant-in-aid from Indian Council of Medical Research (ICMR), Government of India awarded to PS.

Disclosure The authors declare that there is no conflict of interests regarding the publication of this article.

References

1. Paule B, Brion N (2003)EGF receptors in urological cancer. Molecular basis and therapeutic involvements. In: Annales de médecine interne. p 448

Author's personal copy

2. Di Lorenzo G, Tortora G, D'Armiento FP, De Rosa G, Staibano S, Autorino R, D'Armiento M, De Laurentiis M, De Placido S, Catalano G (2002) Expression of epidermal growth factor receptor correlates with disease relapse and progression to androgen-independence in human prostate cancer. Clin Cancer Res 8(11): 3438–3444
3. Traish A, Morgentaler A (2009) Epidermal growth factor receptor expression escapes androgen regulation in prostate cancer: a potential molecular switch for tumour growth. Br J Cancer 101(12): 1949–1956. doi:10.1038/sj.bjc.6605376
4. Sharma SV, Bell DW, Settleman J, Haber DA (2007) Epidermal growth factor receptor mutations in lung cancer. Nat Rev Cancer 7(3):169–181. doi:10.1038/nrc2088
5. Scagliotti GV, Selvaggi G, Novello S, Hirsch FR (2004) The biology of epidermal growth factor receptor in lung cancer. Clin Cancer Res 10(12):4227s–4232s
6. Buck E, Gokhale PC, Koujak S, Brown E, Eyzaguirre A, Tao N, Lerner L, Chiu MI, Wild R, Epstein D (2010) Compensatory insulin receptor (IR) activation on inhibition of insulin-like growth factor-1 receptor (IGF-1R): rationale for cotargeting IGF-1R and IR in cancer. Mol Cancer Ther 9(10):2652–2664. doi:10.1158/1535-7163.MCT-10-0318
7. Singh P, Alex JM, Bast F (2014) Insulin receptor (IR) and insulin-like growth factor receptor 1 (IGF-1R) signaling systems: novel treatment strategies for cancer. Med Oncol 31(1):1–14. doi:10.1007/s12032-013-0805-3
8. Giudice J, Leskow FC, Arndt-Jovin DJ, Jovin TM, Jares-Erijman EA (2011) Differential endocytosis and signaling dynamics of insulin receptor variants IR-A and IR-B. J Cell Sci 124(5):801–811. doi:10.1242/jcs.076869
9. Avnet S, Sciacca L, Salerno M, Gancitano G, Cassarino MF, Longhi A, Zakikhani M, Carboni JM, Gottardis M, Giunti A (2009) Insulin receptor isoform A and insulin-like growth factor II as additional treatment targets in human osteosarcoma. Cancer Res 69(6):2443–2452. doi:10.1158/0008-5472.CAN-08-2645
10. Zhang H, Fagan DH, Zeng X, Freeman KT, Sachdev D, Yee D (2010) Inhibition of cancer cell proliferation and metastasis by insulin receptor downregulation. Oncogene 29(17):2517–2527. doi:10.1038/onc.2010.17
11. Vincent EE, Elder DJ, Curwen J, Kilgour E, Hers I, Tavaré JM (2013) Targeting non-small cell lung cancer cells by dual inhibition of the insulin receptor and the insulin-like growth factor-1 receptor. PLoS One 8(6), e66963. doi:10.1371/journal.pone.0066963. Print 2013
12. Frasca F, Pandini G, Scalia P, Sciacca L, Mineo R, Costantino A, Goldfine I, Belfiore A, Vigneri R (1999) Insulin receptor isoform A, a newly recognized, high-affinity insulin-like growth factor II receptor in fetal and cancer cells. Mol Cell Biol 19(5):3278–3288
13. Pandini G, Frasca F, Mineo R, Sciacca L, Vigneri R, Belfiore A (2002) Insulin/insulin-like growth factor I hybrid receptors have different biological characteristics depending on the insulin receptor isoform involved. J Biol Chem 277(42):39684–39695
14. Hendrickson AEW, Haluska P, Schneider PA, Loegering DA, Peterson KL, Attar R, Smith BD, Erlichman C, Gottardis M, Karp JE (2009) Expression of insulin receptor isoform A and insulin-like growth factor-1 receptor in human acute myelogenous leukemia: effect of the dual-receptor inhibitor BMS-536924 in vitro. Cancer Res 69(19):7635–7643. doi:10.1158/0008-5472.CAN-09-0511
15. Bianco R, Melisi D, Ciardiello F, Tortora G (2006) Key cancer cell signal transduction pathways as therapeutic targets. Eur J Cancer 42(3):290–294. doi:10.1016/j.ejca.2005.07.034
16. Singh P, Bast F (2014) Multitargeted molecular docking study of plant-derived natural products on phosphoinositide-3 kinase pathway components. Med Chem Res 23(4):1690–1700. doi:10.1007/s00044-013-0774-2
17. Singh P, Bast F (2014) In silico molecular docking study of natural compounds on wild and mutated epidermal growth factor receptor. Med Chem Res 23:5074–5085. doi:10.1007/s00044-014-1090-1
18. Phillips P, Sangwan V, Borja-Cacho D, Dudeja V, Vickers S, Saluja A (2011) Myricetin induces pancreatic cancer cell death via the induction of apoptosis and inhibition of the phosphatidylinositol 3-kinase (PI3K) signaling pathway. Cancer Lett 308(2):181–188. doi:10.1016/j.canlet.2011.05.002
19. Sun F, Zheng XY, Ye J, Wu TT, Jl W, Chen W (2012) Potential anticancer activity of myricetin in human T24 bladder cancer cells both in vitro and in vivo. Nutr Cancer 64(4):599–606. doi:10.1080/01635581.2012.665564
20. Zhang X, Chen S, Tang L, Shen Y, Luo L, Xu C, Liu Q, Li D (2013) Myricetin induces apoptosis in Hepg2 cells through Akt/P70s6k/Bad signaling and mitochondrial apoptotic pathway. Anticancer Agents Med Chem 13(10):1575–1581
21. Lee KW, Kang NJ, Rogozin EA, Kim H-G, Cho YY, Bode AM, Lee HJ, Surh Y-J, Bowden GT, Dong Z (2007) Myricetin is a novel natural inhibitor of neoplastic cell transformation and MEK1. Carcinogenesis 28(9):1918–1927
22. Singh P, Bast F (2015) High-throughput virtual screening, identification and in vitro biological evaluation of novel inhibitors of signal transducer and activator of transcription 3. Med Chem Res. doi:10.1007/s00044-015-1328-6
23. da Rocha AB, Lopes RM, Schwartsmann G (2001) Natural products in anticancer therapy. Curr Opin Pharmacol 1(4):364–369
24. Sunil H (2012) Inhibition studies of naturally occurring terpene based compounds with cyclin-dependent kinase 2 enzyme. J Comput Sci Syst Biol 5:2
25. Sarkar FH, Li Y (2006) Using chemopreventive agents to enhance the efficacy of cancer therapy. Cancer Res 66(7):3347–3350
26. Hillman GG (2012) Dietary agents in cancer chemoprevention and treatment. J Oncol. doi:10.1155/2012/749310
27. Phosrithong N, Ungwitayatorn J (2010) Molecular docking study on anticancer activity of plant-derived natural products. Med Chem Res 19(8):817–835
28. Cho JY, Park J (2008) Contribution of natural inhibitors to the understanding of the PI3K/PDK1/PKB pathway in the insulin-mediated intracellular signaling cascade. Int J Mol Sci 9(11): 2217–2230
29. Friesner RA, Murphy RB, Repasky MP, Frye LL, Greenwood JR, Halgren TA, Sanschagrin PC, Mainz DT (2006) Extra precision glide: docking and scoring incorporating a model of hydrophobic enclosure for protein-ligand complexes. J Med Chem 49(21):6177–6196
30. Halgren TA, Murphy RB, Friesner RA, Beard HS, Frye LL, Pollard WT, Banks JL (2004) Glide: a new approach for rapid, accurate docking and scoring. 2. Enrichment factors in database screening. J Med Chem 47(7):1750–1759
31. Friesner RA, Banks JL, Murphy RB, Halgren TA, Klicic JJ, Mainz DT, Repasky MP, Knoll EH, Shelley M, Perry JK (2004) Glide: a new approach for rapid, accurate docking and scoring. 1. Method and assessment of docking accuracy. J Med Chem 47(7):1739–1749
32. Shivakumar D, Williams J, Wu Y, Damm W, Shelley J, Sherman W (2010) Prediction of absolute solvation free energies using molecular dynamics free energy perturbation and the OPLS force field. J Chem Theory Comput 6(5):1509–1519
33. Jorgensen WL, Maxwell DS, Tirado-Rives J (1996) Development and testing of the OPLS all-atom force field on conformational energetics and properties of organic liquids. J Am Chem Soc 118(45):11225–11236
34. Jorgensen WL, Tirado-Rives J (1988) The OPLS [optimized potentials for liquid simulations] potential functions for proteins, energy minimizations for crystals of cyclic peptides and crambin. J Am Chem Soc 110(6):1657–1666

Author's personal copy

35. Lu JJ, Crimin K, Goodwin JT, Crivori P, Orrenius C, Xing L, Tandler PJ, Vidmar TJ, Amore BM, Wilson AG (2004) Influence of molecular flexibility and polar surface area metrics on oral bioavailability in the rat. J Med Chem 47(24):6104–6107
36. Jorgensen WL, Duffy EM (2002) Prediction of drug solubility from structure. Adv Drug Deliv Rev 54(3):355–366
37. Mechoulam H, Pierce EA (2005) Expression and activation of STAT3 in ischemia-induced retinopathy. Invest Ophthalmol Vis Sci 46(12):4409–4416
38. Shih Y-W, Wu P-F, Lee Y-C, Shi M-D, Chiang T-A (2009) Myricetin suppresses invasion and migration of human lung adenocarcinoma A549 cells: possible mediation by blocking the ERK signaling pathway. J Agric Food Chem 57(9):3490–3499
39. Tzeng T-F, Liou S-S, Liu I-M (2011) Myricetin ameliorates defective post-receptor insulin signaling via β-endorphin signaling in the skeletal muscles of fructose-fed rats. Evid Based Complement Alternat Med 2011:150752. doi:10.1093/ecam/neq017
40. Liu I-M, Tzeng T-F, Liou S-S, Lan T-W (2007) Myricetin, a naturally occurring flavonol, ameliorates insulin resistance induced by a high-fructose diet in rats. Life Sci 81(21):1479–1488
41. Simon AR, Rai U, Fanburg BL, Cochran BH (1998) Activation of the JAK-STAT pathway by reactive oxygen species. Am J Physiol-Cell Physiol 275(6):C1640–C1652
42. Walker SR, Nelson EA, Zou L, Chaudhury M, Signoretti S, Richardson A, Frank DA (2009) Reciprocal effects of STAT5 and STAT3 in breast cancer. Mol Cancer Res 7(6):966–976
43. Kumamoto T, Fujii M, Hou D-X (2009) Myricetin directly targets JAK1 to inhibit cell transformation. Cancer Lett 275(1):17–26
44. Morales P, Haza AI (2012) Selective apoptotic effects of piceatannol and myricetin in human cancer cells. J Appl Toxicol 32(12):986–993
45. Safina A, Sotomayor P, Limoge M, Morrison C, Bakin AV (2011) TAK1–TAB2 signaling contributes to bone destruction by breast carcinoma cells. Mol Cancer Res 9(8):1042–1053
46. Gomes LR, Terra LF, Wailemann RA, Labriola L, Sogayar MC (2012) TGF-β1 modulates the homeostasis between MMPs and MMP inhibitors through p38 MAPK and ERK1/2 in highly invasive breast cancer cells. BMC Cancer 12(1):26
47. Dumont N, Arteaga CL (2003) Targeting the TGFβ signaling network in human neoplasia. Cancer Cell 3(6):531–536
48. Alonso H, Bliznyuk AA, Gready JE (2006) Combining docking and molecular dynamic simulations in drug design. Med Res Rev 26(5):531–568
49. Gupta GP, Massagué J (2006) Cancer metastasis: building a framework. Cell 127(4):679–695
50. Javelaud D, Mauviel A (2004) Mammalian transforming growth factor-βs: Smad signaling and physio-pathological roles. Int J Biochem Cell Biol 36(7):1161–1165
51. Fortunel NO, Hatzfeld A, Hatzfeld JA (2000) Transforming growth factor-β: pleiotropic role in the regulation of hematopoiesis. Blood 96(6):2022–2036
52. Chang C, Lee S, Yeh S, Chang T (2013) Androgen receptor (AR) differential roles in hormone-related tumors including prostate, bladder, kidney, lung, breast and liver. Oncogene 33(25):3225–3234
53. Lonergan PE, Tindall DJ (2011) Androgen receptor signaling in prostate cancer development and progression. J Carcinog 10(1):20
54. Maggiolini M, Recchia A, Bonofiglio D, Catalano S, Vivacqua A, Carpino A, Rago V, Rossi R, Ando S (2005) The red wine phenolics piceatannol and myricetin act as agonists for estrogen receptor α in human breast cancer cells. J Mol Endocrinol 35(2):269–281
55. Wang Y, Kreisberg JI, Ghosh PM (2007) Cross-talk between the androgen receptor and the phosphatidylinositol 3-kinase/Akt pathway in prostate cancer. Curr Cancer Drug Targets 7(6):591–604
56. Naderi A, Hughes-Davies L (2008) A functionally significant cross-talk between androgen receptor and ErbB2 pathways in estrogen receptor negative breast cancer. Neoplasia (NY) 10(6):542
57. Craft N, Shostak Y, Carey M, Sawyers CL (1999) A mechanism for hormone-independent prostate cancer through modulation of androgen receptor signaling by the HER-2/neu tyrosine kinase. Nat Med 5(3):280–285
58. Lee AV, Cui X, Oesterreich S (2001) Cross-talk among estrogen receptor, epidermal growth factor, and insulin-like growth factor signaling in breast cancer. Clin Cancer Res 7(12):4429s–4435s
59. Levin ER (2003) Bidirectional signaling between the estrogen receptor and the epidermal growth factor receptor. Mol Endocrinol 17(3):309–317
60. Sak K (2014) Cytotoxicity of dietary flavonoids on different human cancer types. Pharmacogn Rev 8(16):122
61. Labbé D, Provençal M, Lamy S, Boivin D, Gingras D, Béliveau R (2009) The flavonols quercetin, kaempferol, and myricetin inhibit hepatocyte growth factor-induced medulloblastoma cell migration. J Nutr 139(4):646–652